Research Article Vol. 32, No. 11 / 20 May 2024 / Optics Express 19458
Optics EXPRESS

Photoinduced carrier transfer dynamics in a monolayer MoS_2/PbS quantum dots heterostructure

BEN LIU, JINHAI SI,* LIHE YAN, YANAN SHEN, AND XUN HOU

Key Laboratory for Physical Electronics and Devices of the Ministry of Education & Shaanxi Key Lab of Photonic Technique for information, School of Electronics Science & Engineering, Faculty of Electronic and Information Engineering, Xi'an Jiaotong University, Xi'an, 710049, China
*jinhaisi@mail.xjtu.edu.cn

Abstract: Two-dimensional molybdenum disulfide (MoS_2) has been proven to be a candidate in photodetectors, and MoS_2/lead sulfide (PbS) quantum dots (QDs) heterostructure has been used to expand the optical response wavelength of MoS_2. Time-resolved pump-probe transient absorption measurements are performed to clarify the carrier transfer dynamics in the MoS_2/PbS heterostructure. By comparing the carrier dynamics in MoS_2 and MoS_2/PbS under different pump wavelengths, we found that the excited electrons in PbS QDs can transfer rapidly (<100 fs) to MoS_2, inducing its optical response in the near-infrared region, although the pump light energy is lower than the bandgap of MoS_2. Besides, interfacial excitons can be formed in the heterostructure, prolonging the lifetime of the excited carriers, which could be beneficial for the extraction of the carriers in devices.

1. Introduction

Photodetectors with broadband optical response spectra ranging from ultraviolet to near-infrared are widely used in fields of optical communication, thermal imaging, night vision and medical imaging [1–4]. Most traditional broadband photodetectors use single crystal semiconductors, such as Si and InGaAs, which have complex preparation processes, rigidity and brittleness [5,6]. Two-dimensional (2D) transition metal halides (TMDs) are expected to be widely used as the next generation of optoelectronic devices due to their excellent electronic and optical properties [7–10]. As an representative of the TMDs family, molybdenum disulphide (MoS_2) has been mostly explored because of its high carrier mobility and excellent stability [11,12]. Monolayer MoS_2 exhibits a direct bandgap of ~1.8 eV and strong light-matter interaction, making it a promising photoelectric application material [13,14]. Yin et al. firstly reported a novel phototransistor based on mechanically exfoliated monolayer MoS_2 nanosheets, which opened an avenue to develop monolayer semiconducting materials for future optoelectronic devices [15]. However, due to the inherent bandgap limitation, the spectral detection of monolayer MoS_2 photodetectors is usually limited to the ultraviolet to visible light range [16,17]. In order to obtain a broadband photodetector based on monolayer MoS_2, it is a common method to form a vertical heterostructure between MoS_2 and other 2D materials through van der Waals interaction [18,19]. For example, Ding et al. constructed a monolayer MoS_2/2-H $MoTe_2$ heterostructure with a broadband photoresponse with good optical sensitivity ranging from the 200 nm to 1100 nm [20]. Long et al. successfully fabricated and atomically thin MoS_2-graphene-WSe_2 heterostructure which showed broadband photoresponse in the visible to infrared range at room temperature [21].

However, for a certain 2D materials, its bandgap is determined, and the band alignment of the heterostructures formed with MoS_2 is fixed. The bandgap of quantum dots (QDs) can be controlled by tuning the QDs size and have strong and broadband light absorption [22]. For instance, the absorption band edge of PbS QDs can be adjusted from 600 nm to 3000 nm by

#521726 https://doi.org/10.1364/OE.521726
Journal © 2024 Received 16 Feb 2024; revised 29 Apr 2024; accepted 1 May 2024; published 13 May 2024

Optics EXPRESS

controlling the size during the synthesis process [23]. However, the low carrier mobility in PbS QDs blocks their application as photodetectors [24]. MoS_2/PbS QDs hybrid can combine the advantages of the high carrier mobility of the MoS_2 and the strong and tunable light harvesting of PbS QDs [25,26]. For example, Kufer et al. reported a highly sensitive MoS_2/PbS QDs hybrid phototransistor device, which showed several orders of magnitude higher responsivity than that achieved individually by PbS QDs and MoS_2-based photodetectors. Moreover, its spectral detection range has been extended to near-infrared [27]. Besides the extension of the absorption of materials, excited carriers transfer plays important roles in the improvements of the optical responsivity of heterostructures. Although some ultrafast spectroscopy techniques have been used to study these processes [26], deeper understanding the charge transfer and recombination dynamics in heterostructures are needed for the optimization of the devices.

In this work, we studied the carrier dynamics of monolayer MoS_2 and MoS_2/PbS heterostructure using femtosecond pump-probe transient absorption (TA) spectroscopy. We studied the transfer process of interfacial carriers under different energy pump light. We found that when the pump light energy is lower than the bandgap of monolayer MoS_2, the electrons in PbS_2 QDs transferred to MoS_2; when the pump light energy is higher than the bandgap of monolayer MoS_2, the excited holes in MoS_2 transferred to PbS QDs. Besides, interfacial excitons can be formed in the heterostructure prolonging the lifetime of the excited carriers, which could be beneficial for the extraction of the carriers in devices.

2. Materials and methods

2.1. Synthesis of MoS_2/PbS heterostructures

Monolayers MoS_2 films were prepared by chemical vapor deposition (CVD) on 1 mm sapphire substrates (Sixcarbon Technology). PbS QDs with an averaged diameter of about 4 nm were obtained from Mesolight Inc. (Suzhou, China). Toluene (≥99.5%) was purchased from Sinopharm Chemical Reagent Co., Ltd. Acetonitrile (99%) was purchased from Macklin. 1,2-ethanedithiol (99%) was purchased from Macklin. All chemicals were used without further purification. PbS QDs were distributed in toluene with concentrations of 40 mg/mL. Figure 1(a) shows a schematic of the MoS_2/PbS heterojunction preparation process. In order to deposit the PbS QDs on MoS_2 monolayers, 12 μL of the solution were deposited on MoS_2 monolayers using spin coating at 2500 rpm for 15 s. For the purpose of exchanging with the as-synthesized oleic ligand in the pristine PbS QDs, a solution of 1,2-ethanedithiol (EDT) diluted to a concentration 0.02 vol% in acetonitrile (ACN) was dropped on top of the PbS QDs film and left for 30 s before the spin coating. After rotating at 2500 rpm for 15 s, the samples were washed three times with acetonitrile and dried in vacuum. The concentration of PbS QDs on the surface of MoS_2 was estimated to be about $4.2 \times 10^{12}\,cm^{-2}$.

2.2. Instruments and measurements

The Ultraviolet-visible (UV-vis) absorption spectra were obtained from a spectrophotometer (UV-2600, China) and the photoluminescence (PL) spectra were taken with a spectrophotometer (FLS980, Edinburgh). The Raman spectra were acquired from a Raman System (HR800, France) with 532 nm laser excitation. X-ray Photoelectron Spectroscopy (XPS) experiments were carried out with an X-ray photoelectron spectrometer (ESCALAB Xi+, USA).

The TA spectra of the samples were measured using a home-built femtosecond time-resolved TA setup. A mode-locked Ti: sapphire amplifier system with a central wavelength of 800 nm (Vitesse, Conherent, 1 kHz rate, 50 fs pulse with) was used as the laser source. The output was split into two beams, the stronger one was frequency-doubled to produce 400 nm pump light, and the repetition rate was modulated to 500 Hz using an optical chopper. Another beam is focused into the sapphire plate to generate broadband supercontinuum probe light (range from 450 nm to

Optics EXPRESS

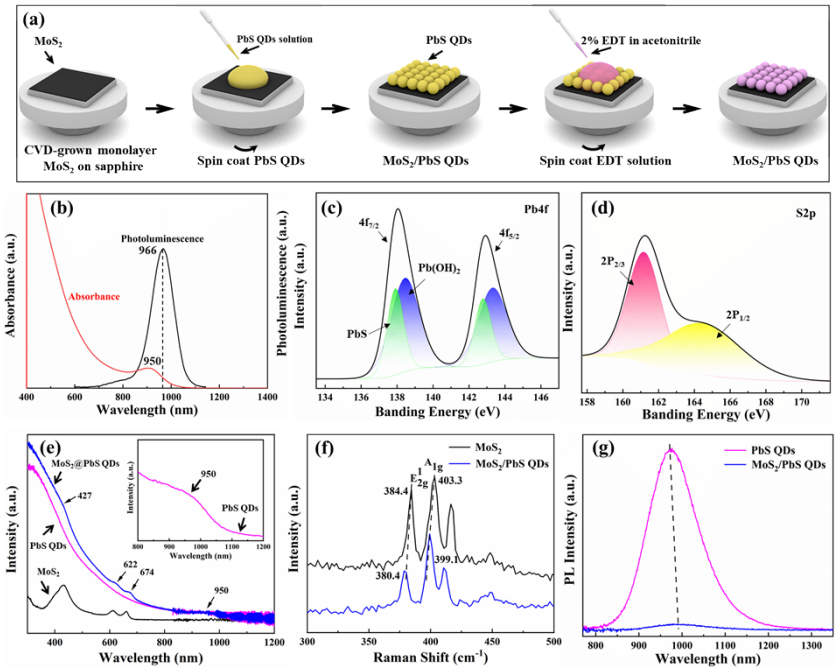

Fig. 1. (a) Schematic diagram of the MoS_2/PbS heterojunction preparation process. (b) Absorbance and photoluminescence spectra of PbS QDs in solution. (c) The XPS Pb4f spectra of PbS QDs thin film. (d) The XPS S2p spectra of PbS QDs thin film. (e) Steady-state absorption spectra of MoS_2 (black), PbS QDs (pink) and MoS_2/PbS heterojunction (blue). (f) Raman spectra of the MoS_2 before and after spin-coating PbS QDs. (g) Photoluminescence spectra of the PbS QDs film (pink) and the MoS_2/PbS heterojunction (blue).

980 nm). The probe light and the pump light were well focused and overlapped on the sample. The TA spectrum was obtained by comparing the probe spectra with and without pump light excitation. By adjusting the delay time between the pump and probe pulses, the variation of the TA spectrum with the delay time was recorded.

Time-resolved two-color pump-probe spectroscopy used the 800 nm fundamental frequency light and the 400 nm doubled frequency laser mentioned above as the pump light, and modulated the frequency to 500 Hz using an optical chopper. The output with different wavelength from the OPA was used as the probe light. Then, the pump pulse and probe pulse were simultaneously focused into the sample, and the pump-probe time delay was controlled using a motorized translation stage. The time-resolved transmission signal was measured by a photodetector and a lock-in amplifier. The time resolution of the femtosecond pump-probe transient absorption system is about 100 femtoseconds. The above experiments were performed with the sample in ambient conditions at room temperature. In the TA and pump-probe measurements, all experiments were conducted below the laser damage threshold of the samples.

3. Result and discussion

3.1. Characterization of materials

We firstly characterized the PbS quantum dots. Figure 1(b) shows the Vis-NIR absorption and PL spectra of PbS QDs in solution, in which an excitonic absorption edge at 950 nm and a PL peak centered at 966 nm can be observed. Figure 1(c) and (d) show the XPS spectra of PbS film. The Pb4f signal contains two peaks corresponding to the spin orbit interactions for the $4f_{7/2}$

Optics EXPRESS

and $4f_{5/2}$ core electronic states. These two peaks are clearly both broad and asymmetric, with shoulders corresponding to peak splitting due to perturbations from the local chemical bonding. The $4f_{7/2}$ peak can be fitted with two components centered at 137.8 eV and 138.4 eV. The former corresponds to the binding energy of Pb-S, while the latter is due to the presence of $Pb(OH)_2$ species at the surface of the PbS QDs [28,29]. The S2p signal contains two peaks corresponding to the $2p_{2/3}$ peak at 161.1 eV and $2p_{1/2}$ peak at 164.5 eV respectively. The $2p_{2/3}$ peak is attributed to S bound to Pb, and the $2p_{1/2}$ peak is assigned to S involved in S-S bonds [30].

Figure 1(e) shows the absorption spectra of monolayer MoS_2, PbS QDs and MoS_2/PbS QDs heterojunction. The strong absorption at three different wavelengths in MoS_2 represents the absorption of A (662 nm), B (610 nm), C (427 nm) excitons, respectively [31,32]. The PbS QDs absorption spectrum (pink line) reveals an absorption peak at 950 nm, as shown in inset of Fig. 1(e). The absorption range of MoS_2/PbS QDs heterojunction ranges from ultraviolet to near-infrared. Its absorption spectrum includes the absorption peaks of MoS_2 and PbS QDs, and the intensity of the absorption peaks is stronger than that of pure MoS_2. We attribute this to the strong absorption and wide absorption range of PbS QDs.

In order to better explore the charge transfer between MoS_2 and PbS QDs, we performed Raman spectroscopy and fluorescence spectroscopy measurements. The Raman spectra of the monolayer MoS_2 before and after spin-coating PbS QDs are shown in Fig. 1(f). The two main peaks located at 384.4 and 403.3 cm^{-1} are attributed to the $E_{2g}{}^1$ (in-plane) and A_1 g (out-of-plane) modes in MoS_2. The difference between the two peaks (18.9 cm^{-1}) is less than 21 cm^{-1}, indicating that the MoS_2 film is monolayer [33]. In the MoS_2/PbS QDs heterojunction, the $E_{2g}{}^1$ and A_1 g phonon frequencies decrease by 4.0 and 4.2 cm^{-1}, respectively. A_1 g phonon have a stronger coupling to electrons than $E_{2g}{}^1$ phonon in monolayer MoS_2 [34]. Thus, the more redshift of the A_1 g indicates electron doping caused by PbS QDs. Figure 1 g shows the PL spectra of the PbS QDs on sapphire substrate and MoS_2. The PL intensity of PbS QDs on MoS_2 is lower than that on the sapphire substrate. The results indicate that most photogenerated electrons in PbS QDs are injected into the MoS_2.

3.2. TA spectra of MoS_2 and MoS_2/PbS

In order to further investigate the carrier transfer process between MoS_2 and PbS quantum dots, we conducted femtosecond time-resolved TA tests on MoS_2 and MoS_2/PbS, respectively. The TA spectrum of MoS_2 is shown in Fig. 2(a), with two valleys located at 615 nm and 660 nm, respectively, corresponding to the ground state bleaching (GSB) signals of B excitons and A excitons. The three peaks are located at 480 nm, 636 nm, and 685 nm, respectively, corresponding to the excited state absorption signals of C excitons, B excitons, and A excitons. The TA spectrum measured using 400 nm light excitation of MoS_2/PbS is shown in Fig. 2(b). Both MoS_2 and PbS can be excited and the characteristic TA signals of MoS_2 can still be observed. As the MoS_2/PbS QDs heterojunction had a strong absorption of white light, the detected transmitted white light intensity in the range of 450 nm to 500 nm was very weak and fluctuated sharply, and the TA signal of MoS_2 at 480 nm cannot be distinguished. Furthermore, we used 800 nm excitation light to only excite PbS, and measured the MoS_2/PbS TA spectrum as shown in Fig. 2(c). As the excitation energy is lower than the bandgap of MoS_2, no signal can be observed in pure MoS_2 film (as shown by the inset of Fig. 2(c)). However, the signal of MoS_2 can still be detected in the MoS_2/PbS QDs heterojunction, indicating that the carrier transfer of PbS to MoS_2 has caused a change in the absorption intensity of MoS_2 of the probe light. The TA spectra measured using 400 nm light excitation of PbS QDs spin-coated on a sapphire plate is shown in Fig. 2(d). The ground state bleaching signal located at 950 nm can be observed, corresponding to the UV absorption peak of PbS QDs.

Optics EXPRESS

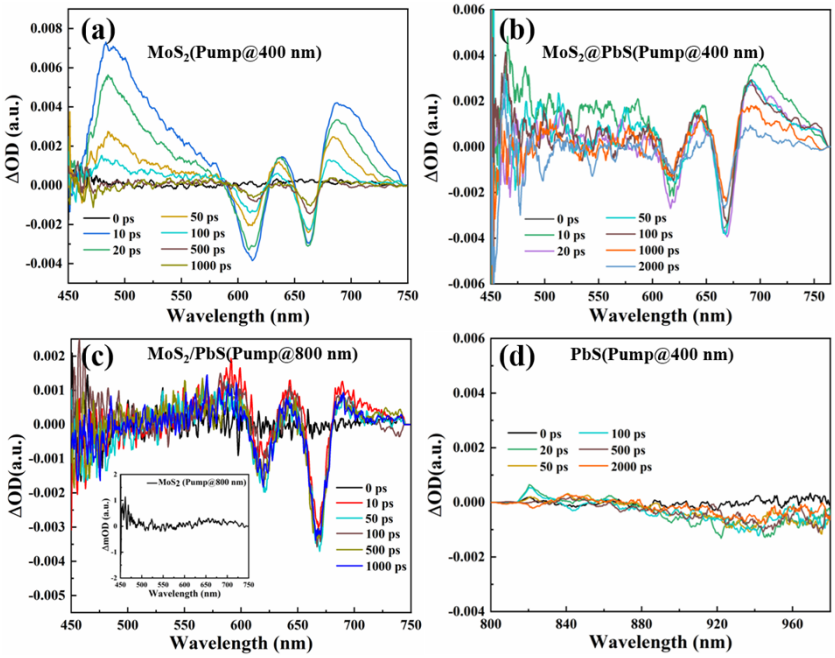

Fig. 2. (a) Femtosecond TA spectra of monolayer MoS_2 with 400 nm excitation. (b) Femtosecond TA spectra of MoS_2/PbS heterostructure with 400 nm excitation. (c) Femtosecond TA spectra of MoS_2/PbS heterostructure with 800 nm excitation. Inset of c shows the femtosecond TA spectra of monolayer MoS_2 with 800 nm excitation. (d) Femtosecond TA spectra of PbS QDs with 400 nm excitation.

3.3. *Charge transfer between MoS_2 and PbS QDs*

As the signal-to-noise ratio of dynamic curve obtained from TA measurements is very low, it's hard to compare the detailed decay processes, especially for those excited by 800 nm laser pulses. In order to compared the excited carrier dynamics under different excitation conditions, the two-color pump-probe spectrum is used to investigate the excited carrier transfer process in MoS_2/PbS heterostructure. Here, probe light of 615 nm laser from the OPA and pump light of the fundamental 800 nm and frequency doubled 400 nm light are used respectively. The 400 nm (3.1 eV) pump pulse is used to excite both the MoS_2 and PbS QDs, while the 800 nm (1.55 eV) pump pulse is used to only excite PbS QDs in the heterostructure.

Figure 3(a) shows the decay process of carrier dynamics in monolayer MoS_2 and MoS_2/PbS heterostructure. The pump and probe wavelength were 400 nm (with a fluence of about 2.6 $\mu J \cdot cm^{-2}$) and 615 nm, respectively. Here, the pump pulse excited both MoS_2 and PbS QDs, and the probe pulse is used to detect photo-generated carriers in MoS_2. There is a long-lived signal lasting about several nanoseconds in pure MoS_2, which could be attributed to the relaxation of excitons bound to defects. [35] As the charge transfer process often takes place in pico-/sub-picosecond regime, we mainly focus the fast rising and decay processes in the first 200 ps. The decay signals of MoS_2 and MoS_2/PbS are well fit using a biexponential decay function (green curves), as shown in Fig. 3(b). The two time constants are $\tau_1 = 2.1 \pm 0.3$ ps (27%), $\tau_2 = 24 \pm 1.2$ ps (73%), respectively. The τ_1 process was extremely rapid, which was caused by charge carriers being trapped by surface trap states. The τ_2 could be attributed to the interband carrier-phonon scattering time [26,36].

Optics EXPRESS

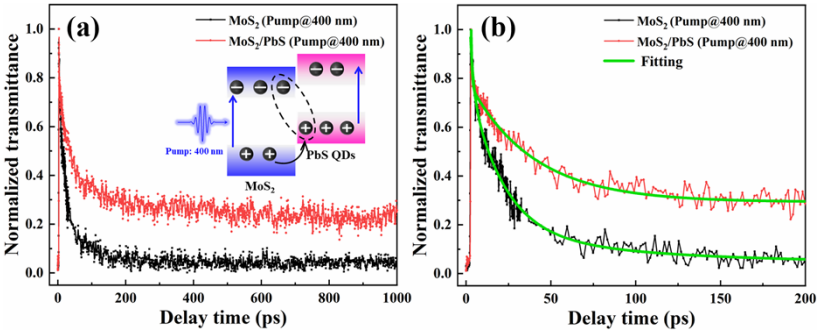

Fig. 3. Normalized time-resolved TA experiment results of monolayer MoS_2 (black squares) and MoS_2/PbS (red circles) heterostructure under 400 nm excitation. (b) Zoomed-in area of (a) for the first 200 ps delay time. The inset is the schematic diagram of hole transfer from MoS_2 to PbS QDs.

The decay signal of MoS_2/PbS is significantly different with that of monolayer MoS_2, which has two time constants in picosecond region as shown in Table 1. The fast decay time $\tau_1 = 0.52 \pm 0.1$ ps (33%) is much faster than pure MoS_2, and we believe that there should be some other process causing the recombination of excited electron and holes. When excited by 400 nm pump light, both MoS_2 and PbS in MoS_2/PbS can be excited as the photon energy of pump pulse is above the band gap of MoS_2. Considering that the band alignment MoS_2 and PbS QDs in heterostructure forms a type II heterojunction [37] (as shown by inset of Fig. 3(a)), excited holes could transfer from MoS_2 to PbS accelerating the decay process of the GSB signal in MoS_2. In addition, the electrons in the conduction band of MoS_2 and the holes in the valence band of PbS QD form interfacial excitons. The $\tau_2 = 36.2 \pm 1.1$ ps (67%) should be attributed to the existence of the recombination process of interfacial excitons. Besides the difference of fast relaxation processes in the samples, the slow relaxation in MoS_2/PbS is obviously enhanced compared with that in pure MoS_2. As the bonding with PbS might introduce more defects in MoS_2 layer, slow relaxation of the excitons bound to defects becomes more pronounced.

Table 1. Fitting results for the two-color pump-probe experiment under different excitation wavelengths

Samples	τ_1 (ps)	τ_2 (ps)
MoS_2 (Pump@400 nm)	2.1 (27%)	24(73%)
MoS_2/PbS (Pump@400 nm)	0.52(33%)	36.2(67%)
MoS_2/PbS (Pump@800 nm)	31.8	–

To further explore the ultrafast charge-transfer and formation of interfacial exciton, we have investigated the photocarrier dynamics of MoS_2/PbS heterostructure under 800 nm excitation with a fluence of about 5.5 $\mu J \cdot cm^{-2}$. As the excitation energy is below the band gap of monolayer MoS_2, the pump injects electron-hole pairs directly into the PbS QD only. The same 615 nm probe as expected before to primarily is used to detect the photocarriers in MoS_2. We can still observe the relaxation signal of MoS_2 excitons in MoS_2/PbS heterostructure, as shown in the Fig. 4(a) (blue triangle). The carrier dynamics excited at 800 nm is significantly different with that excited at 400 nm, which can be well fitted using a single exponential decay function (as shown by green curves in Fig. 4(b)). The results indicate that excited electrons transfer from PbS QDs to MoS_2 inducing the GSB signal in MoS_2, and the interfacial exciton recombination play a leading role in the decay process (the schematic diagram shown in inset of Fig. 4(a)). The holes in the valence band of PbS QDs and the electrons in the conduction band of MoS_2

Optics EXPRESS

form interfacial excitons. The τ=31.8 ± 1.7 ps is attributed to the existence of the recombination process of interfacial excitons.

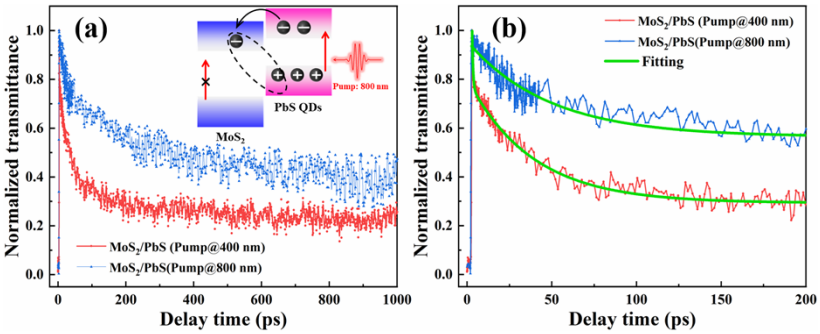

Fig. 4. Normalized time-resolved TR experiment result of monolayer MoS_2/PbS heterostructure under 400 nm (red circles) and 800 nm (blue triangles). (b) Zoomed-in area of (a) for the first 200 ps delay time. The inset is the schematic diagram of electron transfer from PbS QDs to MoS_2.

It should be noted that, the transfer process of the excited electrons could influence the building-up of the TA signal in MoS_2. However, we didn't observe the difference between the rising process of the GSB signals of MoS_2 excited by 400 nm and 800 nm. It may be limited by the temporal resolution (~100 fs) of the measurements, and we believe that transfer of excited electrons from PbS to MoS_2 should be faster than 100 fs. The ultrafast carrier transfer not only ensures that the device has a good photoelectric response for infrared light, but also has an ultrafast optical response.

4. Conclusion

In summary, we have investigated the charge transfer dynamics in MoS_2/PbS QDs heterostructure using femtosecond time-resolved TA and Time-resolved two-color pump-probe spectroscopy techniques. We studied the mechanism of carrier transfer by adjusting the excitation wavelength. Upon excitation above MoS_2 band gap, excited holes in MoS_2 can transfer to PbS QDs, resulting in the formation of interfacial excitations with electron in MoS_2. By comparing the carrier dynamics in MoS_2 and MoS_2/PbS under different pump wavelength, we found that the excited electrons in PbS QDs can transfer rapidly (<100 fs) to MoS_2 inducing its optical response in the near-infrared region, although the pump light energy is lower than the bandgap of MoS_2. Besides, interfacial excitons can be formed in the heterostructure prolonging the lifetime of the excited carriers, which could be beneficial for the extraction of the carriers in devices.

Funding. National Natural Science Foundation of China (62027822); National R&D Program of China (2019 YFA0706402).

Disclosures. The authors declare no conflicts of interest.

Data availability. Data underlying the results presented in this paper are not publicly available at this time but may be obtained from the authors upon reasonable request.

References

1. G. Konstantatos, "Current status and technological prospect of photodetectors based on two-dimensional materials," Nat. Commun. **9**(1), 5266 (2018).
2. D.-S. Um, Y. Lee, S. Lim, *et al.*, "InGaAs nanomembrane/Si van der Waals heterojunction photodiodes with broadband and high photoresponsivity," ACS Appl. Mater. Interfaces **8**(39), 26105–26111 (2016).
3. H. Chen, H. Liu, Z. Zhang, *et al.*, "Nanostructured photodetectors: from ultraviolet to terahertz," Adv. Mater. **28**(3), 403–433 (2016).

Optics EXPRESS

4. X. Gong, M. Tong, Y. Xia, *et al.*, "High-detectivity polymer photodetectors with spectral response from 300 nm to 1450 nm," Science **325**(5948), 1665–1667 (2009).
5. Z. Cheng, T. Zhao, and H. Zeng, "2D material-based photodetectors for infrared imaging," Small Science **2**(1), 2100051 (2021).
6. X. Wu, C. Luo, P. Hao, *et al.*, "Probing and manipulating the interfacial defects of InGaAs dual-layer metal oxides at the atomic scale," Adv. Mater. **30**(2), 1703025 (2017).
7. M. Long, P. Wang, H. Fang, *et al.*, "Progress, challenges, and opportunities for 2D material based photodetectors," Adv. Funct. Mater. **29**(19), 1803807 (2018).
8. M. Zeng, Y. Xiao, J. Liu, *et al.*, "Exploring two-dimensional materials toward the next-generation circuits: from monomer design to assembly control," Chem. Rev. **118**(13), 6236–6296 (2018).
9. H.-P. Komsa and A. V. Krasheninnikov, "Two-dimensional transition metal dichalcogenide alloys: stability and electronic properties," J. Phys. Chem. Lett. **3**(23), 3652–3656 (2012).
10. Z. Sun, A. Martinez, and F. Wang, "Optical modulators with 2D layered materials," Nat. Photonics **10**(4), 227–238 (2016).
11. W. Zhu, T. Low, Y.-H. Lee, *et al.*, "Electronic transport and device prospects of monolayer molybdenum disulphide grown by chemical vapour deposition," Nat. Commun. **5**(1), 3087 (2014).
12. O. Lopez-Sanchez, D. Lembke, M. Kayci, *et al.*, "Ultrasensitive photodetectors based on monolayer MoS_2," Nat. Nanotechnol. **8**(7), 497–501 (2013).
13. A. Splendiani, L. Sun, Y. Zhang, *et al.*, "Emerging photoluminescence in monolayer MoS_2," Nano Lett. **10**(4), 1271–1275 (2010).
14. B. Radisavljevic, A. Radenovic, J. Brivio, *et al.*, "Single-layer MoS_2 transistors," Nat. Nanotechnol. **6**(3), 147–150 (2011).
15. Z. Yin, H. Li, H. Li, *et al.*, "Single-layer MoS_2 phototransistors," ACS Nano **6**(1), 74–80 (2012).
16. S. Manzeli, D. Ovchinnikov, D. Pasquier, *et al.*, "2D transition metal dichalcogenides," Nat. Rev. Mater. **2**(8), 17033 (2017).
17. W. Tang, C. Liu, L. Wang, *et al.*, "MoS_2 nanosheet photodetectors with ultrafast response," Appl. Phys. Lett. **111**(15), 1 (2017).
18. Y. Liu, N. O. Weiss, X. Duan, *et al.*, "Van der Waals heterostructures and devices," Nat. Rev. Mater. **1**(9), 16042 (2016).
19. K. S. Novoselov, A. Mishchenko, A. Carvalho, *et al.*, "2D materials and van der Waals heterostructures," Science **353**(6298), 1 (2016).
20. Y. Ding, N. Zhou, L. Gan, *et al.*, "Stacking-mode confined growth of 2H-$MoTe_2$/MoS_2 bilayer heterostructures for UV-vis-IR photodetectors," Nano Energy **49**, 200–208 (2018).
21. M. Long, E. Liu, P. Wang, *et al.*, "Broadband photovoltaic detectors based on an atomically thin heterostructure," Nano Lett. **16**(4), 2254–2259 (2016).
22. T. Shen, F. Li, Z. Zhang, *et al.*, "High-performance broadband photodetector based on monolayer MoS_2 hybridized with environment-friendly $CuInSe_2$ quantum dots," ACS Appl. Mater. Interfaces **12**(49), 54927–54935 (2020).
23. I. Moreels, Y. Justo, B. De Geyter, *et al.*, "Size-tunable, bright, and stable PbS quantum dots: a surface chemistry study," ACS Nano **5**(3), 2004–2012 (2011).
24. G. Konstantatos and E. H. Sargent, "Nanostructured materials for photon detection," Nat. Nanotechnol. **5**(6), 391–400 (2010).
25. S. Zhang, X. Wang, Y. Chen, *et al.*, "Ultrasensitive hybrid MoS_2-ZnCdSe quantum dot photodetectors with high gain," ACS Appl. Mater. Interfaces **11**(26), 23667–23672 (2019).
26. P. Zereshki, M. M. Tavakoli, P. Valencia-Acuna, *et al.*, "Observation of charge transfer in mixed-dimensional heterostructures formed by transition metal dichalcogenide monolayers and PbS quantum dots," Phys. Rev. B **100**(23), 235411 (2019).
27. D. Kufer, I. Nikitskiy, T. Lasanta, *et al.*, "Hybrid 2D-0D MoS_2-PbS quantum dot photodetectors," Adv. Mater. **27**(1), 176–180 (2015).
28. L. Yan, R Patterson, W Cao, *et al.*, "Air-stable PbS quantum dots synthesized with slow reaction kinetics via a $PbBr_2$ precursor," RSC Adv. **5**(84), 68579–68586 (2015).
29. R. Abargues, J. Navarro, P. J. Rodríguez-Cantó, *et al.*, "Enhancing the photocatalytic properties of PbS QD solids: the ligand exchange approach," Nanoscale **11**(4), 1978–1987 (2019).
30. V. Malgras, A. Nattestad, Y. Yamauchi, *et al.*, "The effect of surface passivation on the structure of sulphur-rich PbS colloidal quantum dots for photovoltaic application," Nanoscale **7**(13), 5706–5711 (2015).
31. Y. Xu, L. Yan, J. Si, *et al.*, "Nonlinear absorption properties and carrier dynamics in MoS_2/graphene van der Waals heterostructures," Carbon **165**, 421–427 (2020).
32. B. Liu, L. Yan, J. Si, *et al.*, "Ultrafast photoinduced carrier transfer dynamics in monolayer MoS_2/graphene heterostructure," J. Appl. Phys. **134**(21), 1 (2023).
33. X Yong, Z Wang, Y Zhan, *et al.*, "Controllable growth of monolayer MoS_2 by chemical vapor deposition via close MoO_2 precursor for electrical and optical applications," Nanotechnology **28**(8), 084001 (2017).
34. B. Chakraborty, A. Bera, D. V. S. Muthu, *et al.*, "Symmetry-dependent phonon renormalization in monolayer MoS_2 transistor," Phys. Rev. B **85**(16), 161403 (2012).

Optics EXPRESS

35. S. Kar, Y. Su, R. R. Nair, *et al.*, "Probing photoexcited carriers in a few-layer MoS_2 laminate by time-resolved optical pump–terahertz probe spectroscopy," ACS Nano **9**(12), 12004–12010 (2015).
36. H. Shi, R. Yan, S. Bertolazzi, *et al.*, "Exciton dynamics in suspended monolayer and few-layer MoS_2 2D crystals," ACS Nano **7**(2), 1072–1080 (2013).
37. O. Özdemir, I. Ramiro, S. Gupta, *et al.*, "High sensitivity hybrid PbS CQD-TMDC photodetectors up to 2 μm," ACS Photonics **6**(10), 2381–2386 (2019).